

Different Compositions of Niobium Titanate (Nb_2TiO_7): Transparent Conducting Oxide Coating for Enhancing the Efficiency of Solar Cell

K. Jasmitha

Centre of Excellence,
Department of Nano-Technology,
Andhra University College of Engineering (A),
Andhra University, Visakhapatnam 530013, India.

Prof.P.Mallikarjuna Rao

Centre of Excellence,
Department of Nano-Technology,
Andhra University College of Engineering (A),
Andhra University, Visakhapatnam 530013, India.

S. Pradeep

Centre of Excellence,
Department of Nano-Technology,
Andhra University College of Engineering (A),
Andhra University, Visakhapatnam 530013, India.

Prof. P.S. Avadhani

Centre of Excellence,
Department of Nano-Technology,
Andhra University College of Engineering (A),
Andhra University, Visakhapatnam 530013, India.

ABSTRACT:

In this project, it is proposed to synthesize and fabricate Anti-Reflective Coating for Solar Cells by using high reproducibility, low material wastage, low contamination growth technique such as E-Beam deposition and synthesize using cost effective and easy processed Top-Down Approach Ball Mill for Niobium Titanate to regain its anatase phase. Hence, to prove the high transmittance, low absorbability and good conductivity which can compensate the existing standard solar cell. The composite was analyzed by XRD, UV Visible spectrometer, FESEM and EDX. Thin film that was deposited is characterized by FESEM, Four Probe Test method and AFM. XRD results were analyzed by using MATCH3! Software, confirmed by comparing the standard JCPD data to figured out the Crystalline Size, Composition, Phase, Structure and density. UV Spectrophotometer gives Absorbance, Transmittance, Reflectance and Bandgap while AFM yields Surface Roughness, Thickness, Topology, Morphology. To check the grain size topography, dislocations cracks in the films FESEM was used. Elemental composition informs the percentage of elements present in the given sample. Niobium Titanate is synthesized with different molar ratios of Niobium dioxide doped in titanium dioxide and ball milled at 3hr, 4hr, 5hr and all these samples was annealed at 500°C for an hour for perfect stoichiometry. The synthesized

powder is made into a pellet and fabricated by high vacuum at 10^{-6} mbar rate of deposition of $\sim (7-10)$ n/S with thickness of 100nm on Si, FTO, Glass using E-Beam deposition technique.

1. Introduction:

Dye-sensitized solar cells (DSSCs) have received great attention due to the low cost and ease of its fabrication process as well as its high power conversion efficiency [1, 2]. A typical DSSC consists of multiple components i.e. transpiring conducting glass which usually utilizes fluorine-doped tin oxide (FTO) or indium-doped tin oxide (ITO), mesoporous metal oxide layer developed from TiO_2 that acts as photoanode, sensitizers (dye molecules), electrolyte (iodide-tri iodide electrolyte is mostly used) and counter electrode. There are several ways to enhance the performance of DSSCs including increasing light harvesting capabilities which can be achieved with good surface area and absorption of broader range of solar light [3], increasing the electron injection speed by improving the electron injection over potential [4, 5], moving the redox couple Fermi level (EF) to enhance the dye regeneration rate [6, 7], enhancing the lifetime of electrons by retarding the probability of charge

Cite this article as: K. Jasmitha, S. Pradeep, Prof.P.Mallikarjuna Rao & Prof. P.S. Avadhani, "Different Compositions of Niobium Titanate (Nb_2TiO_7): Transparent Conducting Oxide Coating for Enhancing the Efficiency of Solar Cell", International Journal & Magazine of Engineering, Technology, Management and Research, Volume 5 Issue 12, 2018, Page 31-42.

recombination [8] and improving the charge transfer rate in TiO_2 [9, 10]. The energy conversion efficiency of DSSCs is determined by the performance of its photoanode. The photoanode supports the sensitizer loading and transfers the photo-excited electrons from the sensitizers to the external circuit. Thus, a large surface area is required to ensure high dye loading. TiO_2 (anatase) has been widely used as photoanode to ensure the transfer of photo-excited electrons. Due to its outstanding optical and electrical properties, TiO_2 has been extensively investigated as one of the most promising wide band gap semiconducting materials in photocatalysis [11, 12] and photovoltaic applications [13]. For instance, TiO_2 with large surface areas are often employed in DSSC [14, 15]. However, its polycrystalline structure results in disordered networks that impede charge transport and lead to the recombination of photo-generated electrons and holes [16]. As a result, single-crystal TiO_2 is preferred as it can provide direct electrical pathways for photo-generated charges and avoid electron scattering or trapping [17]. When electron transport is oriented, the DSSCs can enhance performance in photoelectric conversion. Modification of photoanode in previous studies using TiO_2 based photoanodes has shown that doping with various metals could enhance some of the photovoltaic properties of the cell [18]. There are three main advantages of doping the TiO_2 semiconductor in DSSCs i.e. reduction in band gap which increases the efficiency, reduction in photocatalytic activity of DSSCs and reduction in recombination. Xiang et al. [19] reported the negative shifting of TiO_2 conduction band (CB) as a result of tantalum (Ta) doping; this was due to an increase in open circuit voltage (V_{oc}) which increased the energy conversion efficiency. Kim et al. [20] reported improvements in photoelectric performance of DSSCs using chromium (Cr)-doped TiO_2 semiconductor as photoanode. Zalas et al. [21] studied the influence of rare earth metal doping on the performance of DSSCs; these modified electrodes prevented back transfer of electrons and enhanced dye absorption ability. Lu et al. [9] and Nikolay et al. [22] synthesized niobium (Nb)-doped TiO_2 using the co-hydrolysis method and found an improvement in electron injection and transport

due to the increase in electrical conductivity, shift of EF and conduction band minimum (CBM). However, it is difficult to obtain high crystallinity and size uniformity using the cohydrolysis method; besides that, it also inevitably generates structural defects in TiO_2 which affects the electron injection and transportation [23]. Doping via the co-hydrolysis method also tends to cause deep dopants energy which may not be available for electron injection and transportation. Moreover, the preparation of Nb-doped TiO_2 using the co-hydrolysis method is expensive and niobium chloride (NbCl_5) is unstable and not suitable for use in mass production [9]. Much research has been conducted on the photovoltaic performance of Nb-doped TiO_2 photoanode but its fabrication using the solid state method has not been reported. Fabrication using the solid state method tends to produce a homogeneous powder with high crystallinity structure and is less complicated compared to the co-hydrolysis method. Another important part of DSSC is the sensitizer. The sensitizer is the central component in DSSC as it harvests sunlight and produces photo-excited electrons at the semiconductor interface. There are several requirements for the sensitizer to perform efficiently i.e. chemically adsorbed group to load on the semiconducting material, high molar extinction coefficients in the visible and near-infrared region for light harvesting, and good photostability and solubility to create space between the electrolyte and photoanode for recombination prevention [24]. Various metal complexes and organic dyes have been utilized as sensitizers and the best, to date, is ruthenium-bipyridyl dyes (N719) which display a high energy conversion efficiency of about 11% [25]. In conventional DSSC, ruthenium complexes are the best known, most effective and proven sensitizers. However, ruthenium dye is complicated to synthesize, expensive and not environmentally friendly because of its high toxicity [26-27]. Therefore, a search for novel and alternative dye-sensitizers, especially from natural sources, has become the focus for many researchers [28]; organic dyes containing anthocyanin pigment which is suitable for DSSC applications were extracted from different parts such as the leaves, flowers, fruits and barks of various plants [29-31]. The present work is devoted to

Nb-doped TiO₂ prepared using the solid-state method and its use as a photoanode with dye extracted from *E. conferta* as sensitizer. *E. Conferta* was selected as the sensitizer in this study due to its high acidity and high anthocyanin pigment content which converts light energy into electrical energy. The solid state method is a better approach due to the ease in fabrication as it avoids processes such as pH control and temperature and chemical preparation, and the provision of high sample crystallinity. These advantages induce electron injection and transportation, hence increases the photovoltaic performance. The mechanism provided by Nb doping with *E. conferta* as sensitizer was also investigated based on phase analysis, surface morphology, and electronic and optical behaviors.

2. Experimental Procedure:

2.1. Preparation of Natural Dye Sensitizers

The flesh of *E. conferta* fruits were separated from the seed and completely dried at room temperature. The flesh was crushed to powder form using a mortar. 50 g of the powder was put into a beaker, added with 500 ml ethanol (1:10) and stirred. The mixture was left for 24 hours in the dark at room temperature. The solid residues of the mixture were filtered out to obtain a pure and clear natural dye solution. Further details on the *E. conferta* dye characterization results can be found in our previous work [32].

2.2. Preparation of Nb-doped TiO₂:

TiO₂ doped with 0-2.5 wt% of Nb were synthesized via the solid state method. The mixture was prepared using the ball mixing method. The mixture was filled into 250 ml polyethylene containers with zirconia balls with a ball to powder weight ratio of 10:1. Zirconia balls were used as a mixing media due to its high degree of hardness and to minimize contamination. The containers were placed on the ball mixing roller and mixed for 6 hours at 120 rpm and annealed at 600 °C for 6 hours.

2.3. Preparation of Photoanode and Assembly of DSSCs:

FTO conductive glass with a sheet resistance of ~7Ω/cm²

was cleaned in a detergent solution, rinsed using deionized water and ethanol and then dried. TiO₂ paste was prepared with 0.3 g of TiO₂, 0.5 ml acetic acid, 1:1 (5 ml) mixture of deionized water and ethanol and was ground for 20 minutes. Triton-X was added (0.5 ml) to the mixture and continued to be ground until a homogenous paste was achieved. The TiO₂ pastes were deposited onto FTO glass using the doctor blade technique. The coated films were sintered at 450 °C for 30 minutes. The same method was applied for the 1 wt%, 1.5wt%, 2wt% and 2.5 wt% Nb-doped TiO₂, respectively. The sintered photoanode electrodes were immersed in *E. Conferta* dye solution for 24 hours at room temperature. The sensitized electrodes were rinsed using ethanol to remove unanchored dye. The counter electrode was obtained according to methods employed in previous work [32]. A drop of redox electrolyte was cast on the surface of the sensitized photoanodes. The counter electrode was then clipped onto the top of TiO₂ working electrode with a cell active area of 6.5 cm², and then sealed using slurry tape.

2.4. Cell Characterization

The Fourier transform infrared (FTIR) spectra of dye extracts and dye adsorbed TiO₂ films were measured using a Shimadzu FTIR spectrometer (IRAffinity-1) in the wave number range of 4000–500 cm⁻¹ with a maximum resolution of 0.5 cm⁻¹. Phase identification of the nanomaterials were studied using Bruker D8 Advance which was operated in Bragg Brentano geometry and exposed to CuKα radiation (λ = 1.540Å). The X-ray diffraction (XRD) pattern was scanned with step size of 0.02° (2θ) at a fixed counting time of 71.6 s from 10° to 90° 2θ. The resulting powder diffraction patterns were analyzed using Highscore Plus software. UV-Vis (HP 8453) was used to determine the absorption spectra of all samples. Surface morphology analysis of the samples was carried out using FESEM (Zeiss Supra 35VP) at 5 kV. The photocurrent–voltage (J–V) curves of DSSCs were recorded with a computer-controlled digital source meter (Keithley 2400) under an irradiation of 100 mWcm⁻². The Brunauer–Emmett–Teller (BET) surface area of undoped and Nb-doped TiO₂ powder samples were measured using a surface area analyzer (Micromeritics ASAP 2020). The charge-transfer resistance of a DSSC

was analyzed by electrochemical impedance spectroscopy (EIS, GamryREF 3000, USA) under a light intensity of 100 mW cm⁻² in a frequency ranging from 0.1 Hz to 100 kHz with an AC amplitude of 10 Mv

3. Results and Discussion:

3.1. FTIR Spectra:

The FTIR spectra recorded in the range of 4000 to 500 cm⁻¹ for E. Conferta is shown in Fig. 1. The spectra displayed characteristic vibration at 880 cm⁻¹ which normally occurs in between the standard range of 450 – 1000 cm⁻¹ [33]. The spectra band appearing at 1666 cm⁻¹ for E. conferta corresponds to the C=O (carbonyl) stretching vibrations. Based on Fig. 1, the display of broad absorption in the range of 3000 – 3600 cm⁻¹ with a wide and strong band at 3336 cm⁻¹ indicates the extracted pigments from anthocyanin. The peaks were attributed to –OH stretching and the wide variety of hydrogen bonds between OH. Sharp peaks at 2974 cm⁻¹ and a small shoulder at 2884 cm⁻¹ corresponds to the –CH stretching modes. The peak at 1380 cm⁻¹ was assigned to the asymmetric –CH deformation modes of CH₃ group while peaks 1087 cm⁻¹ and 1046 cm⁻¹ were attributed to C-O vibrations, respectively.

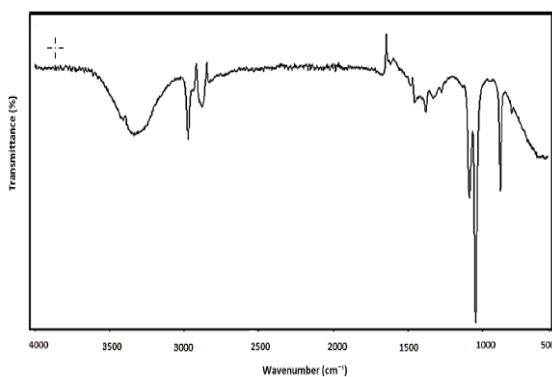


Fig.1. FTIR spectra of extract obtained from E. conferta

3.2. XRD Analysis:

Fig. 2(a) shows the XRD patterns of the undoped TiO₂(0 wt% Nb) and Nb-doped TiO₂ (1.0–2.5 wt% Nb). The peaks indicate that the complete anatase structure after doping with Nb showed no characteristic peaks of Nb₂O₅ in Nb-doped TiO₂ even at 2.5 wt% Nb. In Fig. 2(a), the lattice distortion is due to the defects (vacancies,

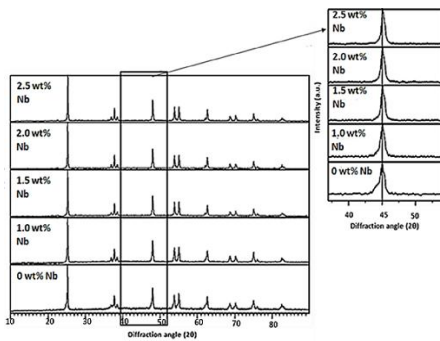
interstitials and substitutions) which can cause shifts in XRD peak positions, depending on the type of strain in the crystal, such as tensile or compressive strain. This shift proves that the Nb⁵⁺ was successfully inserted into the crystal lattice of TiO₂. An observation of the enlarged image shown in Fig. 2(b) indicates a shift in peak positions as well as change in peak broadening. Based on the line from Fig. 2(b), the peaks start to shift when 1 wt% onwards of Nb was doped into the TiO₂. This shows that the Nb doped into the TiO₂ lattice and is evident by the shift in peak position towards a higher angle.. Based on Table 1, it is noticed that the values of lattice constants for 1.0wt% Nb-doped TiO₂ change compared to undoped TiO₂ and increased when the amount of Nb was increased. This is in line with the peak shift, as shown in Fig. 2(b). The crystallite size also increased from 1.0wt% onwards due to change in the fundamental lattice constant as the amount of Nb increases. The cell volume increased from 135.9 Å³ (0 wt% Nb) to 136.5Å³ (2.5 wt% Nb). For Nb doping, the Ti-O bond lengths were slightly extended, and with Nb–O bond lengths being appreciably longer than Ti–O, cell volume of doped TiO₂ was dilated with a rise in local strain field at dopant sites [35].

This can cause a deviation in atomic interactions and promote lattice distortion [36].Therefore, there were significant changes in crystal parameters when the amount of Nb was increased based on lattice constant and crystallite size analysis.

Table 1:Lattice parameter, average crystallite size of Nb-doped TiO₂

Sample	Average crystalline size	Cell volume	a (Å)	c (Å)
0 wt% Nb	8.51	135.9	3.784	9.49
1wt% Nb	11	136.3	3.785	9.50
1.5 wt% Nb	11	136.3	3.785	9.50
2.0 wt% Nb	11.61	136.5	3.786	9.51
2.5 wt% Nb	11.61	136.5	3.786	9.51

(a)



(b)

Fig.2. (a) XRD patterns of 0-2.5wt% Nbdoped TiO₂ and (b) Shifts in peak position and changes in peak broadening are depicted through enlarged view of (020) peaks for undoped TiO₂ and Nb-doped TiO₂.

3.3. Optical Properties Analysis:

To properly investigate the behavior of the Nb-doped TiO₂, the optical properties were studied to understand the photoanode characteristics which are represented in Fig. 3. Based on Fig. 3, the increase of Nb amount doped into TiO₂ significantly expands the absorption spectrum window where strong absorption happens between 300 nm to 450 nm. By comparing 0 wt% Nbdoped TiO₂ (undoped TiO₂) with 1.0 wt%, 1.5 wt%, 2.0 wt% and 2.5wt% Nb-doped TiO₂, the window of absorption spectrum for doping samples was found to have widened. Meanwhile, the absorption peaks for 1.0 wt% and 1.5 wt% Nb-doped TiO₂ were higher compared to 0wt% Nbdoped TiO₂. The samples with wide absorption spectrum and higher peaks gave advantages to the photovoltaic performance of the system [37]. However, when the amount of dopants increased, the peak absorbance of the samples decreased. Fig. 3 indicates that when the Nb dopant amount increased, the absorbance intensity of visible light increased. The absorption edge that shifts towards the longer wavelength indicates an increase in the band gap of the DSSC. The results of the optical band gap (E_g) illustrated in Fig. 4 was calculated using the UV-vis spectra, as shown in Eq. 1: $n = (1 - \alpha) / (\alpha h\nu - A)$ where α is the optical absorption coefficient, $h\nu$ is the photon energy, E_g is the absorption band gap, A and n are constants. For the indirect

semiconductor of anatase TiO₂, n is equal to 2 [38]. Therefore, the tangent intercept in the plot of $2(1/h\nu)\alpha$ versus $h\nu$ that represents the E_g is shown in Fig. 4. The band gap decreased when the Nb dopant increased i.e., from 3.34 eV to 3.06 eV, 3.14 eV, 3.20 eV and 3.22 eV, for 0 wt% Nb 1.0 wt% Nb, 1.5 wt% Nb, 2.0 wt% Nb and 2.5 wt% Nb, respectively. By doping Nb into TiO₂, the incorporation of Nb⁵⁺ into TiO₂ lattice forms an intraband state making a positive shift of conduction band minimum (CBM)[39]. Therefore, higher absorbance can be seen in the Nb-doped TiO₂ film due to smaller band gap. The decrease in band gap is also due to the decrease in the bottom of the TiO₂ conduction band which narrowed the band gap and improved driving force of injected electron resulting in increased TiO₂ (e-) concentration and absorbance after doping Nb.

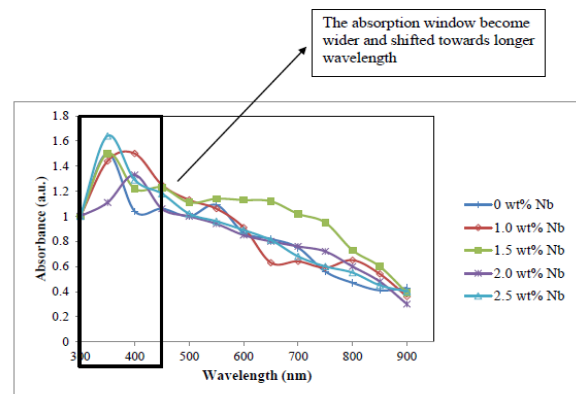


Fig. 3. The UV-vis absorbance spectra of DSSC based on Nb-doped TiO₂ with different Nb amounts

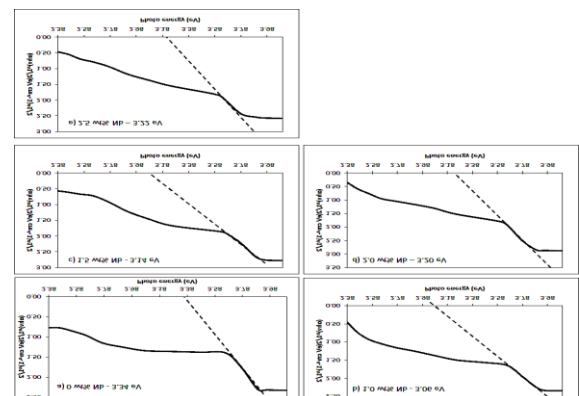


Fig.4. Plots of $(ah\nu)^{1/2}$ versus photon energy for Nb-doped TiO₂ at (a) 0 wt% Nb (b) 1.0 wt% Nb (c) 1.5 wt% Nb (d) 2.0 wt% Nb (e) 2.5 wt% Nb

3.4. Surface morphology analysis

The effects of doping concentration on surface morphology is shown in Fig. 5. With reference to the surface morphology image in the film, a uniform coating displaying the absence of voids and dense morphology for the entire substrate surface area can be observed. The solid-state technique of pulverization was employed to initiate doping with subsequent sintering; this facilitates the formation of an oxide network which can act as a pathway for charge transport [41]. Sintering greatly influences charge transportation. It can be seen that 0 wt%, 1.0 wt%, 1.5 wt% and 2.5 wt% Nb films produced homogenous spherical shaped crystals. At 1.0 wt% Nb and 1.5 wt% Nb, a continuous and dense morphology was observed with small porous structure; films with denser structure and smooth surface were produced at these concentrations. As the Nb dopants increased to 2.5 wt%, the surface of the film became denser and agglomeration of grains was observed. Aggregated and uneven distribution of grains was also observed when the amount of Nb dopants increased. This is due to increase in stress developed during deposition and growth process which can be related to the different ionic radius of Nb⁵⁺ and Ti²⁺. The formation of spherical structure allows scattering of incident light which increases photon travelling distance thus confining the incident light within them to enhance electron conduction and reduction of photon loss [42, 43]. The small particles can absorb enough dye while the spaces between spheres facilitate the permeation of the electrolyte while the bigger particles enhance light scattering which improves the efficiency of D.

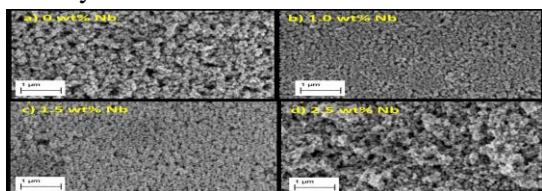


Fig.5. Surface morphology images for Nb-doped TiO₂ at (a) 0 wt% Nb (b) 1.0 wt% Nb (c) 1.5 wt% Nb (d) 2.5 wt% Nb

Grain size was measured using ASTM E112-12 and based on Fig. 6, the grain decreased from 131.3 nm to

126.5 nm for 0 wt% to 1.0 wt% of Nb and increased to 128.4 nm and 134.0 nm for 1.5 wt% to 2.5 wt% of Nb, respectively. Grain growth inhibitions also affected the increase in band gap. When the Nb content was increased, the particle size became smaller which led to smaller band gap energy [45], as shown in Fig 6. The effect of change in band gap energy with respect to particle size is that the bulk defects induce delocalization of molecular orbitals in the conduction band, create deep traps in electronic energy and increases the band gap [46].

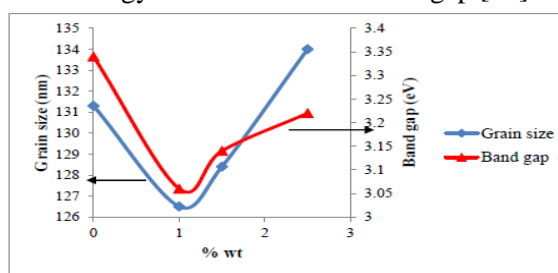


Fig.6. Correlation between grain size and band gap energy

3.5. Photovoltaic performance of DSSC

In order to determine the photovoltaic performance, the current density–voltage (J–V) curves of DSSC based on undoped and Nb-doped TiO₂ electrodes with different amounts of Nb dopant are shown in Fig. 7 and the photovoltaic properties are shown in Table 2.

The photovoltaic performance of DSSC based on Nb-doped TiO₂ electrodes showed improvement with 1.0 wt% to 2.5 wt% of Nb dopant. The highest efficiency was obtained with 1.0 wt% Nb dopant which is 1.40 % compared to standard DSSC photoanodes i.e. 0 wt% Nb. This is followed by 1.5 wt% Nb which produced 1.23%, 2.0 wt% Nb produced 1.07 % and 2.5 wt% Nb produced 0.95 % .The increase in efficiency of doped photoelectrode compared to pure photoelectrode may be due to the amount of dye molecules chemisorbed onto doped TiO₂ which is much higher than the amount chemisorbed onto pure TiO₂ [47].The short-circuit photocurrent density (J_{sc}) is the one of the important aspect in photovoltaic parameters. The high J_{sc} reflects the enhancement of electron injection and transport based on the shifted CBM and improved the electron

conductivity. The highest JSC for DSSC was displayed by 1.0 wt% Nb content with a value of 5.00 mA/cm². The increase in Jsc can be related to the decrease in the band gap of Nb-doped TiO₂, as shown in Fig. 4. The decrease in the band gap of the Nb-doped TiO₂ to visible region causes photoexcitation which leads to an increase in electron hole pairs.

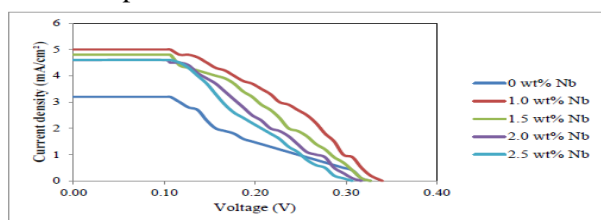


Fig.7. The photocurrent density–photovoltage (J–V) of the fabricated DSSC using undoped (0 wt% Nb) and Nb-doped TiO₂ (1.0-2.5 wt% Nb)

Table 2: Lattice parameter, average crystallite size of Nb-doped TiO₂

Sample	J _s (mA/m ²)	Voc/V	Efficiency(%)	Surface area
0 wt% Nb	3.20	0.32	0.80	6.1407
1.0 wt% Nb	5.00	0.33	1.40	8.8314
1.5 wt% Nb	4.80	0.32	1.23	7.3451
2.0 wt% Nb	4.60	0.31	1.07	-
2.5 wt% Nb	4.60	0.30	0.95	-

The electrons can be pumped directly from the intermediate band (IB) to the conduction band (CB) or from the valance band (VB) to the IB, and finally to the CB. Therefore, this increases the photoelectron density in CB and also increases the Jsc[48]. The influence of Nb doping on Voc is that it combines energy difference between the Fermi level (EF) of the electrodes and the

redox potential of the electrolyte. The decreased difference between the positive shift EF of Nb-doped TiO₂ and the redox potential of I⁻/I₃⁻ couple decreases the Voc[50]. The electron density increases with the occurrence of photoexcitation at the semiconductor and enhances the photo-injection contribution. The appropriate morphology which is provided by optimum porosity also enhances the improvement in surface area, as shown in Table 2. The surface area increased from 6.14 m²/g to 8.83 m²/g when doped with 1.0 wt% Nb and decreased to 7.35 m²/g when amount of dopant was increased. The smaller grain size improves the surface area of the film for effective absorption of dye. Therefore, the increase of surface area enhances the dye absorption and increases the Jsc value. Meanwhile, the decrease in Jsc for samples with higher amounts of Nb dopant is due to the destruction of TiO₂ crystal lattice and the existence of more defects in the crystal lattice which acts as a trapping center of photo generated charge [49]. As shown in Table 2, the highest Voc is found in the DSSC with 1.0wt% Nb-doped TiO₂. The Voc decreased when the amount of Nb increased. The influence of Nb doping on Voc is that it combines energy difference between the Fermi level (EF) of the electrodes and the redox potential of the electrolyte. The decreased difference between the positive shift EF of Nb-doped TiO₂ and the redox potential of I⁻/I₃⁻ couple decreases the Voc[50]. Nb doping also reduces the concentration of oxygen vacancies at the TiO₂ surface. Therefore, the space charge region widened to suppress recombination at the TiO₂–electrolyte interface and leads to the increment of Voc[51]. The decrease in Voc and Jsc is also due to how Nb would have acted as a new recombination center thus reducing the number of charge carriers [52]. Electrochemical impedance spectroscopy (EIS) is a useful method to analyze the kinetics of the electrochemical process in DSSC [53]. EIS measurement was carried out to investigate the TiO₂/dye/electrolyte interfacial charge transfer kinetics. Fig. 8 shows the Nyquist plots for DSSC using undoped and Nb-doped TiO₂ photoanodes. The equivalent circuit is depicted in the inset of Fig. 8. Nyquist plots of DSSC produced two typical semicircles, as shown in Fig. 8, which can be explained by the charge-

transfer resistance at the counter electrode/electrolyte interface (RCE) and at the photoanode/dye/electrolyte interface (RCT)[54, 55]. . The calculated EIS parameters of an equivalent circuit (inset in Fig. 8) for the Nb-doped TiO₂ are given in Table 3. In a DSSC, R_s is related to the collection of electrons from the external circuit [56]. Thus, the difference in the values of R_s was negligible. In Table 3, T0.0Nb shows high electron transport resistance (RCE) compared to other dopants. High RCE values show that there is difficulty in electron transport in the counter electrode which reduced the current density (J_{sc}), while low RCE values for T1.0Nb showed faster electron transport and produced higher J_{sc}.

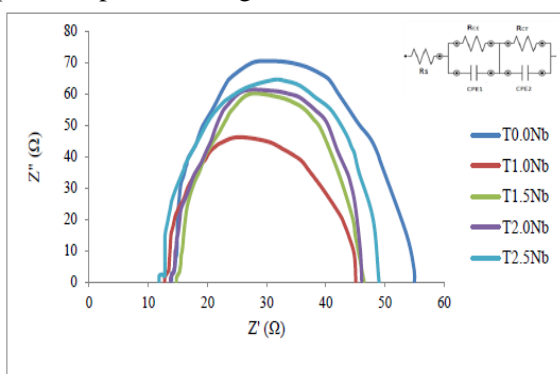


Fig.8. Nyquist plots of DSSCs measured under illumination conditions for undoped and Nb doped TiO₂

Table.3: Properties determined by EIS measurement with different amounts of Nb dopant

Sample	R _s (Ω)	RCE (Ω)	RCT (Ω)
T0.00Nb	13.94	8.66	70.50
T0.00Nb	12.76	2.13	45.00
T0.50Nb	14.76	4.48	60.00
T0.00Nb	13.76	5.34	62.00
T0.50Nb	11.83	5.30	64.50

The charge transfer resistance related to the recombination of electrons (RCT) at the photoanode/dye/electrolyte interface is determined using the semicircles at the intermediate frequency regions. Fig. 8 indicates that when the amount of Nb increased (until T1.0Nb), the radius decreased. The RCT value for T1.0Nb is the lowest compared to other dopants (14.28

Ω). It proves that electron transfer becomes faster within the TiO₂ film, implying that the film conductivity was improved [57]. It also suggests that when the electron gets faster, it provides better charge transfer which improves its capability to hold carriers for a longer time, indicating an increase in the capacitance of the device using Nb-doped TiO₂ which may be contributed to the existence of quantum capacitance [58]. Based on this result, it can be deduced that Nb dopant has improved the capacitance of the device, leading to higher J_{sc} and V_{oc} values. However, when the dopant amount increased (T1.5Nb onwards), the RCT increased due to the formation of more defects in the semiconductor [49]. Higher RCT value corresponds to lower probability in recombination of electrons. The low recombination of electron leads to the decrease in J_{sc} and V_{oc} values due to high recombination process [59].

4. Conclusions

The performance of Nb-doped TiO₂ synthesized using the solid state method as photoanode and E. conferta as sensitizer promoted and favoured electron transformation. The dye-sensitized solar cells (DSSC) with 1.0 wt% Nb-doped TiO₂ improved the J_{sc} and V_{oc} and produced the highest efficiency of about 1.40%. The improvement of J_{sc} is related to the enhancement of electron injection and transportation. The reduction in the concentration of oxygen vacancies at the TiO₂ surface is correlated to Nb doping. Therefore, the space charge region was found to widen up and suppress electron recombination at the TiO₂-electrolyte interface thereby leading to increment in V_{oc}.

References:

- [1] S. Zhang, X. Yang, Y. Numata, L. Han, Highly efficient dye-sensitized solar cells: progress and future challenges, Energy Environ. Sci. 6 (2013) 1443–1464.
- [2] H. Jeong, Y. Pak, Y. Hwang, H. Song, K.H. Lee, H.C. Ko, G.Y. Jung, Enhancing the Charge Transfer of the Counter Electrode in Dye-Sensitized Solar Cells Using Periodically Aligned Platinum Nanocups, Small. 8 (2012) 3757–3761.

- [3] F. Huang, Q. Li, G. J. Thorogood, Y. B. Cheng, R. A. Caruso, Zn-doped TiO₂ in dye-sensitized solar cells for enhanced photocurrent. *J. Mater. Chem.* 22 (2012).
- [4] S. E. Koops, B. C. O' Regan, P. R. F. Barnes, J. D. Durran, Parameters Influencing the Efficiency of Electron injection in Dye Sensitized solar cell, *J. Am. Chem. Soc.* 131 4808-4818.
- [5] Q. Wang, S. Ito, M. Gratzel, F.F Santiago, I. Mora-Sera, J. Bisquert, T. Bessho, H. Imai, Characteristics of high efficiency dye sensitized solar cells, *J. Phys. Chem. B.* 110 25210-25221.
- [6] S.M. Feldt, G. Wang, G. Boschloo, A. Hagfeldt, Effects of Driving Forces for Recombination and Regeneration on the Photovoltaic Performance of Dye-Sensitized Solar Cells using Cobalt Polypyridine Redox Couples, *J. Phys. Chem. C.* 115 (2011) 21500-21507.
- [7] H. Wang, M. Liu, C. Yan, J. Bell, Reduced electron recombination of dye-sensitized solar cells based on TiO₂ spheres consisting of ultrathin nanosheets with [001] facet exposed Beilstein *J. Nanotechnol.* 3 (2012) 378-87.
- [8] F. Fabregat-Santiago, J. Bisquert, G. Garcia-Belmonte, G. Boschloo, A. Hagfeldt, Influence of electrolyte in transport and recombination in dye-sensitized solar cells studied by impedance spectroscopy, *Sol. Energ. Mat. Sol. Cells.* 87 (2005) 117-131.
- [9] X. Lü, X. Mou, J. Wu, D. Zhang, L. Zhang, F. Huang, F. Xu, S. Huang, Improved-Performance Dye-Sensitized Solar Cells Using Nb-Doped TiO₂ Electrodes: Efficient Electron Injection and Transfer, *Adv. Funct. Mater.* 20 (2010) 509-5
- [10] J. Liu, H. Yang, W. Tan, X. Zhou, Y. Lin, Photovoltaic performance improvement of dye-sensitized solar cells based on tantalum-doped TiO₂ thin films, *Electrochim. Acta.* 56(2010) 396-400.
- [11] R. Asahi, T. Morikawa, T. Ohwaki, K. Aoki, Y. Taga, Visible-Light Photocatalysis in Nitrogen-Doped Titanium Oxides, *Science.* 293 (2001).
- [12] B. Tian, X. Zheng, T. J. Kempa, Coaxial silicon nanowires as solar cells and nanoelectronic power sources. *Nature.* 449 (2007) 885-889.
- [13] Y. Duan, N. Fu, Q. Liu, Y. Fang, X. Zhoy, J. Zhang, Y. Lin, Sn-Doped TiO₂ Photoanode for Dye-Sensitized Solar Cells, *J. Phys. Chem. C.* 116 (2012) 8888-8893.
- [14] W. Sun, T. Peng, Y. Liu, Hierarchically porous hybrids of polyaniline nanoparticles anchored on reduced graphene oxide sheets as counter electrodes for dye-sensitized solar cells, *J. Mater. Chem. A.* 1 (2013) 2762-2768.
- [15] Y. Zhao, A. Thapa, Q. Feng, Electrospun TiC/C nano-felt surface-decorated with Pt nanoparticles as highly efficient and cost-effective counter electrode for dye-sensitized solar cells, *Nanoscale.* 5 (2013) 11742-11747.
- [16] Y. Hao, X. Yang, J. Cong, Engineering of highly efficient tetrahydroquinoline sensitizers for dye-sensitized solar cells, *Tetrahedron.* 2 (2012) 552-558.
- [17] Y. Zhou, M. Eck, C. Veit, Efficiency enhancement for bulk-heterojunction hybrid solar cells based on acid treated CdSe quantum dots and low bandgap polymer PCPDTBT, *Sol. Energ. Mat. Sol. Cells.* 4 (2011) 1232-1237.
- [18] S. Shakir, Z. S. Khan, A. Ali, Development of copper doped titania based photoanode and its performance for dye sensitized solar cell applications, *J. Alloy. Comp.* 652 (2015) 331-340.
- [19] P. Xiang, W. Ma, T. Xiao, L. Jiang, X. Tan, T. Shu, Ta-doped hierarchical TiO₂ spheres for dye-sensitized solar cells, *J. Alloy. Comp.* 656 (2016) 45-50.

- [20] C. Kim, K. Sim, H. Kim, Modification of a TiO₂ photoanode by using Cr-doped TiO₂ with an influence on the photovoltaic efficiency of a dye-sensitized solar cell, *J. Mater.Chem.* 18 (2008) 5809-5814.
- [21] M. Zalas, M. Walkowiak, Increase in efficiency of dye-sensitized solar cells by porous TiO₂ layer modification with gadolinium-containing thin layer, *J. Rare Earth.* 8 (2011) 783-786.
- [22] T. Nikolay, L. Larina, O. Shevaleevskiy, B.T. Ahn, Electronic structure study of lightly Nb-doped TiO₂ electrode for dye-sensitized solar cells, *Energy Environ. Sci.* 4 (2011) 1480-1486.
- [23] L. De Trizio, R. Buonsanti, A.M. Schimpf, A. Llordes, D.R. Gamelin, R. Simonutti, D.J. Milliron, Nb-Doped Colloidal TiO₂ Nanocrystals with Tunable Infrared Absorption, *Chem. Mater.* 25 (2013) 3383-3390.
- [24] A. Yella, H. W. Lee, Porphyrin-Sensitized Solar Cells with Cobalt (II/III)-Based Redox Electrolyte Exceed 12 % Efficiency, *Science.* 334 (2011) 629-634.
- [25] M. Gratzel, Conversion of sunlight to electric power by nanocrystalline dye-sensitized solar cells, *J. Photochem. Photobiol. A.* 164(2004) 3-14.
- [26] S. Hao, J. Wu, Natural dyes as photosensitizers for dye-sensitized solar cell, *Sol Energy.* 80(2006) 209-214.
- [27] M. Hamadani, J. Safaei-Ghomi, M. Hosseinpour, R. Masoomi, V. Jabbari, Uses of new natural dye photosensitizers in fabrication of high potential dye-sensitized solar cells (DSSCs), *Mater. Sci. Semicond. Process.* 27 (2014) 733-739.
- [28] A. Ghamdi, R. Gupta, Improved solar efficiency by introducing graphene oxide in purple cabbage dye sensitized TiO₂ based solar cell, *Solid State Commun.* 183 (2014) 56-59.
- [29] H. Chang, Y. Lo, Pomegranate leaves and mulberry fruit as natural sensitizers for dye-sensitized solar cells, *Sol Energy.* 84 (2010) 1833-1837.
- [30] R. Grünwald, H. Tributsch, Mechanisms of instability in Ru-based dye sensitized solar cells. *J. Phys. Chem.* 101 (1997) 2564-2575.
- [31] G. Calogero, G. Marco, Red Sicilian orange and purple eggplant fruits as natural sensitizers for dye-sensitized solar cells, *Sol. Energ. Mat. Sol. Cells.* 92 (2008) 1341-1346.
- [32] J. Hidayani, Y. Madihan, Efficient Dye-Sensitized Solar Cells Using *G. Atroviridis* and *E. Conferta* Fruits, *Australian Journal of Basic and Applied Sciences.* 37 (2015) 367-370.
- [33] K.V. Hemalatha, S.N. Karthick, C. Justin Raj, N.-Y. Hong, S.-K. Kim, H.-J. Kim, Performance of *Kerria japonica* and *Rosa chinensis* flower dyes as sensitizers for dye-sensitized solar cells, *Spectrochim. Acta Mol. Biomol. Spectrosc.* 96 (2012) 305-309.
- [34] A. Sahai, Y. Kumar, V. Agarwal, S. Olive-Méndez, N. Goswami, Doping concentration driven morphological evolution of Fe doped ZnO nanostructures, *J. Appl. Phys.* 116(2014) 164315.
- [35] Z. Zhao, Q. Liu, Effects of lanthanide doping on electronic structures and optical properties of anatase TiO₂ from density functional theory calculation. *J. Phys. D: Appl. Phys.* 41 (2008) 085417.
- [36] P.S. Archana, R. Jose, T. M. Jin, C. Vijila, M. M. Yusoff, S. Ramakrishna, Structural and Electrical Properties of Nb-Doped Anatase TiO₂ Nanowires by Electrospinning, *J. Am. Ceram. Soc.* 93 (2010) 4096-4102.
- [37] G. Zhu, Z. Cheng, T. Lv, Zn-doped nanocrystalline TiO₂ films for CdS quantum dots sensitized solar cells, *Nanoscale.* 2 (2010) 1229-1232.

- [38] B.K. Kaleji, R. Sarraf-Mamoory, A. Fujishima, Influence of Nb dopant on the structural and optical properties of nanocrystalline TiO₂ thin films, *Mater. Chem. Phys.* 132 (2012) 210-215.
- [39] S. Kim, M. Ju, I. Choi, W. Choi, Nb-doped TiO₂ nanoparticles for organic dye-sensitized solar cells, *RSC Adv.* 3 (2013) 16380–16386.
- [40] L. Wei, Y. Yang, X. Xia, R. Fan, T. Su, Y. Shi, J. Yu, L. Li and Y. Jiang, Band edge movement in dye sensitized Sm-doped TiO₂ solar cells: a study by variable temperature spectroelectrochemistry, *RSC Adv.* 5 (2015) 70512-70521.
- [41] N. Chestnoy, T. Harris, R. Hull, Luminescence and photophysics of cadmium sulfide semiconductor clusters: the nature of the emitting electronic state, *J. Phys. Chem.* 90(1986) 3393–3399.
- [42] K. Park, J. Xi, Q. Zhang, G. Cao, Charge Transport Properties of ZnO Nanorod Aggregate Photoelectrodes for DSCs, *J. Phys. Chem. C.* 115 (2011) 20992-20999.
- [43] S. Hore, S. Hore, C. Vetter, R. Kerna, H. Smit, A. Hirsch, Influence of scattering layers on efficiency of dye-sensitized solar cells, *Sol. Energ. Mater. Sol. Cells.* 90 (2006) 1176-1188.
- [44] F. Huang, D. Chen, X. L. Zhang, R. A. Caruso, Y. B. Cheng, Dual-Function Scattering Layer of Submicrometer-Sized Mesoporous TiO₂ Beads for High-Efficiency Dye-Sensitized Solar Cells, *Adv. Funct. Mater.* 20 (2010) 1301-1305.
- [45] Y. Yang, X. Chen, Y. Feng, G. Yang, Physical Mechanism of Blue-Shift of UV Luminescence of a Single Pencil-Like ZnO Nanowire, *Nano Lett.* 7 (12) (2007) 3879-3883.
- [46] H. Lin, C.P. Huang, W. Li, C. Ni, S. Ismat Shah, Y. H. Tseng, Size dependency of nanocrystalline TiO₂ on its optical property and photocatalytic reactivity exemplified by 2-chlorophenol, *Appl. Catal. B.* 68 (2006) 1–11
- [47] P. Manurung, Y. Putri, W. Simanjuntak, Growth and characterization of ZnO nanostructured thin films by a two-step chemical method, *Ceram. Int.* 39(2013) 255-259.
- [48] Y. Zhang, L. Wang, B. Liu, Synthesis of Zn doped TiO₂ microspheres with enhanced photovoltaic performance and application for dye sensitized solar cells, *Electrochim. Acta.* 56 (2011) 6517-6523.
- [49] L. Zhou, L. Wei, Y. Yang, X. Xia, P. Wang, J. Yu, T. Luan, Improved performance of dye sensitized solar cells using Cu-doped TiO₂ as photoanode materials: Band edge movement study by spectroelectrochemistry, *Chem. Phys.* 475 (2016) 1–8.
- [50] L. Souza, R. Shwetharani, V. Amoli, Photoexcitation of Neodymium Doped TiO₂ for Improved Performance in Dye – Sensitized Solar Cells, *Mater. Des.* 104 (2016) 346-354.
- [51] S. Zhang, X. Yang, Y. Numata, L. Han, Highly efficient dye-sensitized solar cells: progress and future challenges, *Energy Environ. Sci.* 6 (2013) 1443–1464.
- [52] L. Wei, X. Xia, Y. Yang, P. Wang, Y. Dong, T. Luan, Variable temperature spectroelectrochemistry study of silver-doped TiO₂ and its influence on the performance of dye sensitized solar cells, *RSC Adv.* 6 (2016) 68341-68350.
- [53] M. Adachi et al., Determination of parameters of electron transport in dye sensitized solar cells using electrochemical impedance spectroscopy, *J. Phys. Chem. B* 28 (2006) 13872–13880.
- [54] C.P. Lee, P.Y. Chen, R. Vittal, K.C. Ho, Iodine-free high efficient quasi solid-state dye sensitized solar cell containing ionic liquid and polyaniline-loaded carbon black, *J. Mater. Chem.* 20 (2010) 2356–2361.



[55] J.K. Koh, J. Kim, B. Kim, J.H. Kim, E. Kim, Highly Efficient, Iodine-Free Dye-Sensitized Solar Cells with Solid-State Synthesis of Conducting Polymers, *Adv. Mater.* 23 (2011) 1641–1646.

[56] J. Jia, J. Wu, J. Dong, P. Zhou, S. Wu, J. Lin, Cobalt selenide/tin selenide hybrid used as a high efficient counter electrode for dye-sensitized solar cells, *J. Mater. Sci. :Mater. Electron.* 26 (2015) 10102.

[57] H. Su, Y. T. Huang, Y. H. Chang, P. Zhai, N. Y. Hau, P. C. H. Cheung, W. T. Yeh, T. C. Wei, S. P. Feng, The Synthesis of Nb-doped TiO₂ Nanoparticles for Improved-Performance Dye Sensitized Solar Cells, *Electrochim. Acta.* 182 (2015) 230–237.

[58] A.A. Shah, A.A. Umar, M.M. Salleh, Efficient Quantum Capacitance Enhancement in DSSC by Gold Nanoparticles Plasmonic Effect, *Electrochim. Acta.* 195 (2016) 134–142.

[59] N. C. D. Nath, H. J. Lee, J. J. Lee, W. Y. Choi, Electrochemical approach to enhance the open-circuit voltage (V_{oc}) of dye-sensitized solar cells (DSSCs), *Electrochim. Acta* 109(2013) 39–45.